PHYSICAL REVIEW B, VOLUME 64, 195133

X-ray resonant scattering studies of orbital and charge ordering in $Pr_{1-x}Ca_xMnO_3$

M. v. Zimmermann,[1] C. S. Nelson,[1] J. P. Hill,[1] Doon Gibbs,[1] M. Blume,[1] D. Casa,[2] B. Keimer,[2] Y. Murakami,[3] C.-C. Kao,[4] C. Venkataraman,[5] T. Gog,[5] Y. Tomioka,[6] and Y. Tokura[6,7]
[1] *Department of Physics, Brookhaven National Laboratory, Upton, New York 11973-5000*
[2] *Department of Physics, Princeton University, Princeton, New Jersey 08544*
and Max-Planck-Institut für Festkörperforschung, 70569 Stuttgart, Germany
[3] *Photon Factory, Institute of Materials Structure Science High Energy Accelerator Research Organization, Tsukuba 305-0801, Japan*
[4] *National Synchrotron Light Source, Brookhaven National Laboratory, Upton, New York 11973-5000*
[5] *CMC-CAT, Advanced Photon Source, Argonne National Laboratory, Argonne, Illinois 60439*
[6] *Joint Research Center for Atom Technology (JRCAT), Tsukuba 305-0033, Japan*
[7] *Department of Applied Physics, University of Tokyo, Tokyo 113-0033, Japan*
(Received 30 August 2000; published 30 October 2001)

We present the results of a systematic x-ray scattering study of the charge and orbital ordering in the manganite series $Pr_{1-x}Ca_xMnO_3$ with $x=0.25$, 0.4, and 0.5. The temperature dependence of the scattering at the charge and orbital wavevectors, and of the lattice constants, was characterized throughout the ordered phase of each sample. It was found that the charge- and orbital-order wavevectors are commensurate with the lattice, in striking contrast to the results of electron and neutron diffraction studies of samples with $x=0.5$. High-momentum-transfer resolution studies of the $x=0.4$ and 0.5 samples further revealed that while long-range charge order is present, long-range orbital order is never established. Above the charge and orbital ordering temperature T_0, the charge-order fluctuations are more highly correlated than the orbital fluctuations. This suggests that charge order drives orbital order in these samples. In addition, a longitudinal modulation of the lattice with the same periodicity as the charge and orbital ordering was discovered in the $x=0.4$ and 0.5 samples. For $x=0.25$, only long-range orbital order was observed with no indication of charge ordering, nor of an additional lattice modulation. We also report the results of a preliminary investigation of the loss of charge and orbital ordering in the $x=0.4$ sample by application of a magnetic field. Finally, the polarization and azimuthal dependence of the charge and orbital ordering in these compounds are characterized both in the resonant and nonresonant limits, and compared with the predictions of current theories. The results are qualitatively consistent with both cluster and local density approximation $+U$ calculations of the electronic structure.

DOI: 10.1103/PhysRevB.64.195133 PACS number(s): 75.30.Vn, 61.10.Eq, 64.60.Cn

I. INTRODUCTION

Interest in the origins of high-temperature superconductivity and colossal magnetoresistance in the transition metal oxides has driven much of the activity currently at the center of condensed matter physics. An important aspect of these strongly correlated electron systems is that no single degree of freedom dominates their response. Rather, the ground state properties are thought to reflect a balance among several correlated interactions, including orbital and charge ordering, magnetism, and coupling to the lattice.

The perovskite manganites provide an especially illuminating example of the interplay among these interactions, since in these materials the balance may be conveniently altered, for example, by doping or through an applied magnetic field.[1] As a result, much work has been done to understand their magnetic ground states and lattice distortions, dating back to the seminal experiments of Wollan and Koehler.[2] Less is known about the roles of charge and orbital order in these materials. The classic work of Goodenough[4] has nevertheless served as a guide to their ordered arrangements, as supplemented, for example, by detailed measurements of the crystal structure and of the temperature dependence of the lattice constants (see Refs. 5and 6, for example).

This situation has changed during the last three years following the detection of orbital order by resonant x-ray scattering techniques.[7–13] Specifically, it has been found that the sensitivity of x-ray scattering to these structures can be significantly enhanced by tuning the incident x-ray energy to the transition metal K absorption edge. Thus, it appears possible to characterize the orbital and charge ordering on a microscopic scale, and to study their response to changes of temperature or to an applied magnetic field. Insofar as we are aware, resonant x-ray scattering studies of these materials have now been extended to include $La_{0.5}Sr_{1.5}MnO_4$,[7] $LaMnO_3$,[8] $La_{1-x}Sr_xMnO_3$,[12,14] $Pr_{1-x}Ca_xMnO_3$,[15] V_2O_3,[16] $YTiO_3$,[17] $LaTiO_3$,[18] $LaSr_2Mn_2O_7$,[19] DyB_2C_2,[20,21] and $Nd_{0.5}Sr_{0.5}MnO_3$,[22,23] and this list continues to grow. There is, in addition, an ongoing discussion of whether it is more appropriate to treat the resonant cross section within an extended, band structure description of the electronic structure, or instead with a more localized, atomic description.[11,24,25,13] A related question concerns how to write the resonant cross section explicitly in terms of the order parameters for orbital and charge ordering.

In this paper, we present x-ray scattering studies of $Pr_{1-x}Ca_xMnO_3$ with $x=0.25$, 0.4, and 0.5. Detailed studies have been made of the temperature dependence of the orbital and charge order scattering of all three samples, including characterization of the intensities, wavevectors, correlation lengths, and lattice constants. Below a doping-dependent ordering temperature T_0, it is found that the charge- and/or orbital-order wavevectors are commensurate with the lattice at all temperatures. This contrasts with the results of other studies where a significant variation of these wavevectors was reported near T_0 (see *Note added in proof* and Refs. 3, 26, 27). Surprisingly, our high-momentum-transfer resolution studies reveal that long-range orbital order is never established in the $x=0.4$ and 0.5 samples, although long-range charge order is observed in both. Further, for temperatures above T_0, the charge order fluctuations are longer ranged than the orbital fluctuations, suggesting that the charge ordering drives the orbital ordering in these systems. Recent Landau theories of the phase transition are consistent with this picture.[28] In contrast, for $x=0.25$ we observe long-range orbital order, with no indication of any charge ordering. We have also monitored the destruction of charge and orbital ordering after the application of a magnetic field in the $x=0.4$ sample. A similar phenomenology is found for increasing magnetic field as occurs for increasing temperature.

Finally, detailed measurements of the polarization and azimuthal dependence of the charge and orbital ordering have been carried out in both the resonant and nonresonant limits. In the $\sigma\rightarrow\pi$ channel at the orbital wavevector of all three samples, we find that the resonant cross section is qualitatively consistent with the results obtained earlier[8] for $LaMnO_3$ and with the predictions of both the localized and band-structure descriptions of the electronic structure. Likewise, we have found that the resonant scattering at the charge order wavevector is consistent with earlier results obtained for $La_{1.5}Sr_{0.5}MnO_4$.[7] We have, in addition, discovered scattering in the $\sigma\rightarrow\sigma$ channel at the charge and orbital wavevectors of the $x=0.4$ and 0.5 samples. On the basis of its polarization and Q dependence, we have deduced that it originates from a longitudinal lattice modulation. Earlier studies of $La_{0.5}Ca_{0.5}MnO_3$ had previously found a transverse modulation,[6,29–31] and a similar modulation had been assumed in $Pr_{1-x}Ca_xMnO_3$. A summary of the present work was published earlier.[15]

The organization of this paper is as follows. The experimental setup is described immediately below, followed by a brief description of charge and orbital ordering in $Pr_{1-x}Ca_xMnO_3$. A simple model of the resonant orbital cross section is given in Sec. IV. Our main results and discussion follow in Sec. V. A brief summary is given at the end.

II. EXPERIMENT

The single crystals used in the present experiments were grown by float zone techniques at the Joint Research Center for Atom Technology (JRCAT). (0,1,0) surfaces were cut from cylinders of radius 3 mm, and polished with fine emery paper and diamond paste. The mosaic widths of the samples as characterized at the (0,2,0) bulk Bragg reflections (in orthorhombic notation) were 0.1°, 0.25°, and 0.25° [full width at half maximum (FWHM)], for the $x=0.25$, 0.4, and 0.5 samples, respectively. These values varied by small amounts as the beam was moved across each sample surface, reflecting its mosaic distribution. The growth techniques and basic transport properties of these crystals have been described in detail elsewhere.[32–34]

Most of the x-ray scattering experiments were carried out at the National Synchrotron Light Source on beam lines X22C, X22B, and X21. The X22C beam line is equipped with a bent, toroidal focusing mirror and a Ge(111) double crystal monochromator arranged in a vertical scattering geometry. This gives an incident linear polarization of 95% (σ) and an incident energy resolution of about 5 eV at the Mn K edge (6.545 keV). Three different detector configurations were used. Low-momentum-transfer resolution scans employed slits before the detector, and provided a longitudinal resolution of 0.0021 $Å^{-1}$ [half width at half maximum (HWHM)] at the (010) reflections of each sample. High-resolution scans employed a standard Ge(111) crystal, and gave a longitudinal resolution of 4.5×10^{-4} $Å^{-1}$ (HWHM) at the respective (010) reflections. The third configuration provided linear polarization analysis of the scattered beam via rotation of a Cu(220) crystal about the scattered beam direction.[35] It gave longitudinal resolutions of 0.0069 $Å^{-1}$ and 0.0052 $Å^{-1}$ (HWHM) in the $\sigma\rightarrow\sigma$ and $\sigma\rightarrow\pi$ geometries, respectively. For an incident photon energy set at the Mn K absorption edge, the Cu(220) scattering angle is 95.6°. This leads to a 5–10 % uncertainty in the polarization-dependent intensities due to incomplete suppression of the unselected component of the scattered beam and the small π component of the incident beam.

Magnetic field experiments were performed at the National Synchrotron Light Source (NSLS) beam line X22B, which supports a bent, toroidal mirror and a single crystal Ge(111) analyzer-monochromator combination. These experiments were carried out in the nonresonant limit, with an incident photon energy of 8 keV. The sample was mounted in a 13 T superconducting magnet oriented in a horizontal scattering geometry. In addition, two series of experiments were performed on the NSLS wiggler beam line X21, which was equipped with a four-bounce Si(220) monochromator and a focusing mirror, leading to an extremely good incident energy resolution of 0.25 eV. Finally, one set of experiments was carried out on undulator beam line 9ID at the Advanced Photon Source. The optics for beam line 9ID were comprised of a double crystal Si(111) monochromator and a flat harmonic rejection mirror.

III. PROPOSED ORBITAL- AND CHARGE-ORDERED STRUCTURES

At room temperature, the crystal structure of $Pr_{1-x}Ca_xMnO_3$ is orthorhombic ($Pbmn$), as illustrated in Fig. 1. Characteristic of the perovskite manganites, each Mn atom lies at the center of the octahedron defined by the oxygen atoms at the corners. Single layers of Pr atoms lie between the layers of octahedra. Depending on the temperature, there may be distortions of the octahedra and tilts as is also illustrated in Fig. 1. The solid line in the figure outlines the orthorhombic unit cell.

A schematic phase diagram for $Pr_{1-x}Ca_xMnO_3$ versus Ca concentration and temperature[5,33] is shown in Fig. 2. For small x ($0.15\leqslant x\leqslant0.3$) and at low temperatures,

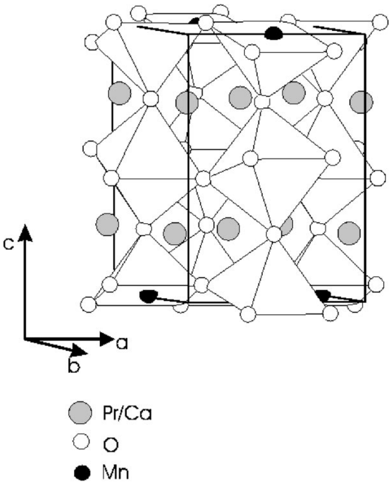

FIG. 1. Schematic structure of $Pr_{1-x}Ca_xMnO_3$. Small spheres correspond to oxygen, and large spheres to Pr or Ca. The Mn atoms are at the center of the octahedra. Solid lines show the orthorhombic unit cell used in this paper.

$Pr_{1-x}Ca_xMnO_3$ is a ferromagnetic insulator, and is believed to exhibit an orbitally ordered ground state analogous to that observed in $LaMnO_3$. The electronic configuration of the Mn^{3+} (d^4) ions is (t_{2g}^3, e_g^1) with the t_{2g} electrons localized at the Mn sites. The e_g electrons are hybridized with the oxygen $2p$ orbitals, and believed to participate in a cooperative Jahn-Teller distortion of the MnO_6 octahedra. This leads to a $(3x^2-r^2)$-$(3y^2-r^2)$-type of orbital order of the e_g electrons in the ab plane with the oxygens displaced along the direction of extension of the e_g orbitals. A schematic illustration of this orbitally ordered state for $x=0.25$ is shown in Fig. 3(a),[5] with the orbital unit cell marked by the solid line. The excess Mn^{4+} ions in this material are believed to be disordered, though recently, other proposals have been put forward.[36–38] It is noteworthy that the orbital period is twice that of the fundamental Mn spacing, so that orbital scattering appears at structurally forbidden reflections. In orthorhombic notation, for which the fundamental Bragg peaks occur at $(0,2k,0)$, the orbital scattering then occurs at $(0,k,0)$.

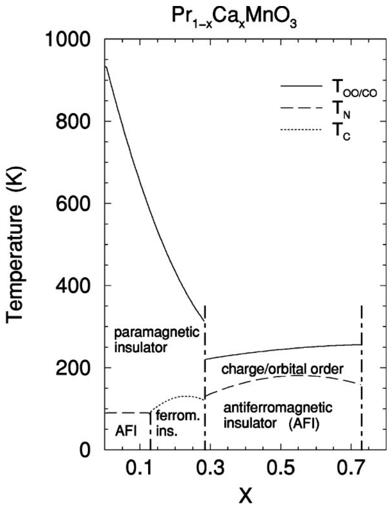

FIG. 2. Composition-temperature phase diagram of $Pr_{1-x}Ca_xMnO_3$ in zero magnetic field (following Ref. 5). The full lines indicate the charge/orbital transition temperature ($T_{OO/CO}$); antiferromagnetic transitions (T_N) are marked with dashed lines and ferromagnetic transitions (T_C) with dotted lines.

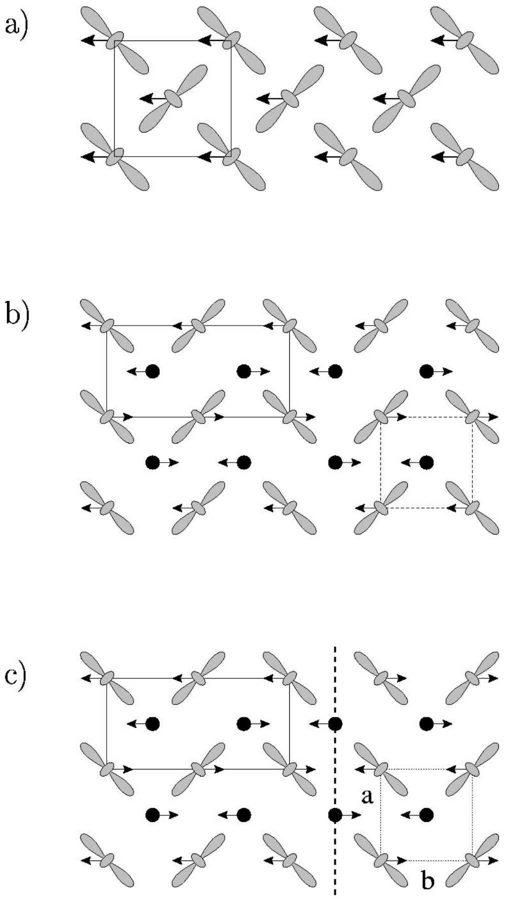

FIG. 3. Schematic of the charge, orbital, and magnetic order in $Pr_{1-x}Ca_xMnO_3$. Filled circles represent Mn^{4+} ions, shaded figure-8's represent Mn^{3+} ions, and the arrows indicate the in-plane components of the magnetic ordering. Solid lines show the orbital-order unit cell; dashed lines show the charge-order unit cell. (a) Proposed orbital ordering for $x=0.25$, (b,c) Charge and orbital order for $x=0.4$ and 0.5, with (c) showing an orbital antiphase domain wall.

Recently, the possibility of the existence of both charge and orbital ordering at $x=0.25$ has been suggested by various theoretical approaches.[36–38] Mizokawa *et al.*[36] studied a related material, $La_{1-x}Sr_xMnO_3$, and found an ordered arrangement of $(3x^2-r^2)$-$(3y^2-r^2)$- and $(3z^2-r^2)$-type orbitals surrounding the Mn^{4+} sites at $x=0.25$. While this structure is inconsistent with the magnetic structure in $Pr_{0.75}Ca_{0.25}MnO_3$, it first raised the possibility of structures other than those proposed by Jirak *et al.*[5] As discussed below, however, we have found no evidence for this type of charge ordering.

For Ca concentrations $0.3 \leqslant x \leqslant 0.7$, $Pr_{1-x}Ca_xMnO_3$ becomes an antiferromagnetic insulator at low temperatures (see Fig. 2), and exhibits colossal magnetoresistance in applied magnetic fields, with the metal-insulator transition occurring between 5 and 8 T.[33] These effects result from charge ordering among the Mn^{3+} and Mn^{4+} ions, which occurs in addition to orbital ordering. The large conductivity is enabled through the hopping of e_g electrons among Mn sites. The fraction of Mn ions in the Mn^{4+} state is determined largely by the concentration of Ca ions. Thus, by varying the Ca concentration, it is possible to alter the balance between charge and orbital ordering. The proposed ground state[5] for both the $x=0.4$ and $x=0.5$ concentrations is shown in Fig. 3(b). The small filled circles represent the Mn^{4+} ions, with one fewer electron than is localized at the Mn^{3+} sites. The solid line indicates the unit cell for orbital ordering, while the dashed line gives that for charge ordering. It is interesting that the proposed structures for $x=0.4$ and 0.5 are identical[5] and commensurate with the lattice, independent of concentration. Clearly, at least for $x=0.4$, this picture cannot be strictly correct. Jirak *et al.* proposed that the extra electrons present at $x=0.4$ could be accommodated in such a structure by a partial occupancy of the $3z^2-r^2$ orbitals of the nominal Mn^{4+} sites. Other possibilities include small Mn^{3+}-rich regions, higher-order structures, or small regions of orbital disorder. As discussed below, our data reveal that, in fact, the orbital order is not long-ranged in either of these compounds, although the charge order is.

In the orthorhombic notation, the charge order reflections occur at $(0,2k+1,0)$ and the orbital order reflections at $(0,k+1/2,0)$. Note that the orbital period $(=2b)$ in the $x=0.4$, 0.5 compounds differs from that occurring in samples with $x<0.3$ $(=b)$, as a result of the presence of charge ordering.

The magnetic structure of these compounds at low doping $(0.15\leqslant x\leqslant 0.3)$ is ferromagnetic with $T_C\approx 140$ K. Compounds with higher doping $(0.3\leqslant x\leqslant 0.75)$ are CE-type antiferromagnets with $T_N=170$ K for x between 0.4 and 0.5.[5] The in-plane components of the magnetic structures are also illustrated in Fig. 3.

IV. RESONANT CROSS SECTION FOR ORBITAL ORDERING: A SIMPLE MODEL

The present experiments were carried out using x-ray resonant scattering techniques. As shown in a series of recent papers,[7–14,22–25] the sensitivity of x-ray scattering to orbital ordering in the transition metal oxides is enhanced when the incident x-ray energy is tuned near the K absorption edge. In the resonant process, a core level electron is promoted to an intermediate excited state, which subsequently decays. This can lead to new scattering mechanisms, such as resonant magnetic scattering. In that case, the excited electron is promoted to a partially occupied orbital and the sensitivity to the magnetic polarization arises through the exchange interaction.[39,40] In the present case, we consider a dipole process involving a Mn $1s$ to $4p$ transition. To understand the origin of the sensitivity to orbital order, we consider a simple model in which it is assumed that the $4p_{x,y,z}$ states are initially unoccupied, but split in the orbitally ordered state (see Fig. 4). This gives rise to a nonzero resonant scattered intensity at reflections sensitive to the difference between the two orbitally ordered sublattices. This model, summarized below, is designed to capture the essence of the problem, but not the details of the interactions for which a more sophisticated theory is required. For example, recent local spin density (LSDA) $+U$ calculations[11] suggest that the $4p$ bands are not split *per se*, but rather experience changes in the weight of the density of states in the ordered phase. Nevertheless, our model is conceptually simple, and reproduces most of the systematics of the data.

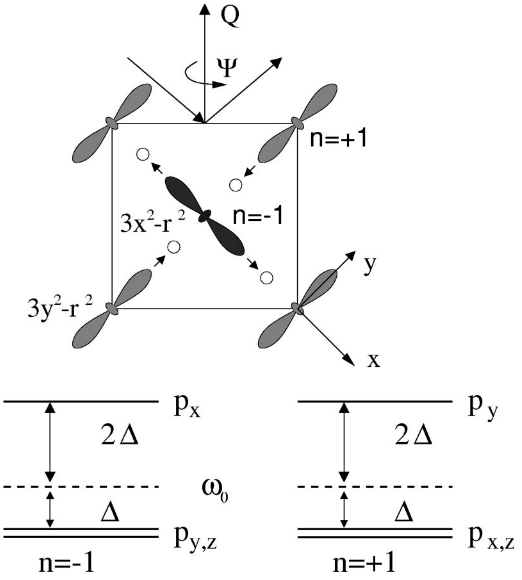

FIG. 4. Upper panel: Schematic view of the orbital in the a-b plane of the $\mathrm{LaMnO_3}$. Lower panel: Schematic energy level diagram of Mn $4p_{x,y,z}$ in the orbitally ordered state, for the two orbital sublattices.

For a difference reflection, the resonant scattered intensity may be written[8]

$$I^{\mathrm{res}}=\sum_{x,y,z,n=\pm 1} n\frac{\langle s|P^{\alpha}|p_m\rangle\langle p_m|P^{\beta}|s\rangle}{\omega-\omega_0-\delta\omega_m^n+i\Gamma/2}\epsilon'^{\alpha}\epsilon^{\beta}, \tag{1}$$

where the coordinate system has been chosen so that x and y are along the direction of extension of the ordered e_g orbitals and z is perpendicular to the x-y plane (see Fig. 4). $|s\rangle$ and $|p\rangle$ are the wave functions of the Mn $1s$ and $4p$ orbitals, respectively. P^{α} is the α component of the dipole operator $(\alpha=x,y,z)$, ω is the incident photon energy, and ω_0 is the energy of the unperturbed p_m levels. The incident (final) polarization of the photons is ϵ (ϵ') and $n=\pm 1$ labels the orbital sublattice. Γ is the lifetime of the excited state. Note, $\langle p_m|P^{\alpha}|s\rangle=A\delta_{m\alpha}$, where A is a constant. As illustrated in the figure, $\delta\omega_m^n=-\Delta$ for $n=+1$, $m=x,z$; $\delta\omega_m^n=2\Delta$ for $n=+1$, $m=y$; and so on.

The origin of the splitting Δ is not specified in our model. Two mechanisms (both consistent with the measurements) have been discussed, and indeed, the discussion has sparked some controversy.[7–14,22–25,41,42] One possible origin involves the Coulomb coupling of the Mn $3d$ and $4p$ levels, either directly or indirectly through the hybridization of the Mn$(3d)$-O$(2p)$ and O$(2p)$-Mn$(4p)$ states.[25] The latter effect has the same sign as the direct Coulomb interaction, but is expected to be smaller.[25] In this picture, the Coulomb coupling raises the $4p_m$ levels lying parallel to the direction of extension of the orbital (by 2Δ in our model) and lowers those lying perpendicular (by Δ) as shown in Fig. 4. Detailed calculations using atomic orbitals by Ishishara and Maekawa[25] have found qualitative consistency with all of the known experimental results for $La_{1-x}Sr_{1+x}MnO_4$,[7] $LaMnO_3$,[8] $Pr_{1-x}Ca_xMnO_3$,[15] and $La_{1-x}Sr_xMnO_3$.[12] Alternatively, the motion of the oxygen atoms away from regions of high charge density through the Jahn-Teller interaction lowers the energy of the $4p_m$ levels lying parallel to the direction of the extension of the orbital, and raises those lying perpendicular. This effect thus has the opposite sign to that of the $3d$-$4p$ Coulomb interaction discussed above, and in fact these mechanisms compete with each other. Several groups have argued that the oxygen motion is the dominant effect leading to resonant scattering at the orbital wavevector.[11,13,24,41,42] Calculations of the resonant cross section based on such approaches, and utilizing band-structure descriptions of the $4p$ density of states in $LaMnO_3$ (which show changes in weight, rather than a simple splitting) also reproduce the main experimental facts and further, make detailed predictions about the resonant fine structure measured in x-ray scattering experiments.[11,15] Insofar as we are aware, the experimental data obtained to date do not distinguish either theoretical approach conclusively, and this remains an open question. For the purpose of calculating the resonant cross section of our simplified model, however, all that is required is that $\Delta \neq 0$.

We stress that regardless of which of the two microscopic mechanisms is the dominant one, the resonant scattering will reflect the symmetry of the orbital ordering through the pertubation of the local electronic states at the Mn^{3+} sites. We believe this is true even though the *d* orbitals are not directly involved as intermediate states in the resonant process. In particular, in terms of the Jahn-Teller distortion considered above, the orientation of the e_g orbitals and the oxygen motion reflect the same order parameter. It follows that the peak positions and widths determined in the x-ray experiments measure the orbital periodicity and correlation lengths, respectively. However, it still remains to interpret the x-ray peak intensities on an absolute scale in terms of the order parameter for orbital ordering, which will require additional calculations. From this perspective, we think of the resonant scattering as Templeton scattering arising from the anisotropic charge distribution induced by orbital ordering. Its basic properties, for example the polarization and azimuthal dependence, are then determined by the anisotropy of the susceptibility tensor, which in the dipole approximation is a second rank tensor.

Working in a linear polarization basis, with σ polarization perpendicular to the scattering plane and π parallel, it is easy to show that for a σ incident beam, the resonant cross section for an orbital reflection of the type considered here, does not give rise to a σ' polarized scattered beam. That is, for any azimuthal angle ψ, $I_{\sigma\to\sigma'}=0$. In the rotated π' channel, it may be further shown that

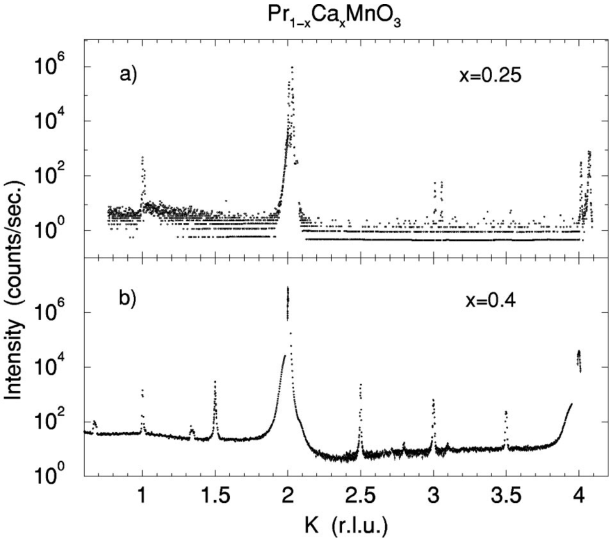

FIG. 5. Upper: Scan along $(0,k,0)$ of the $x=0.25$ sample at $T=300$ K at the resonance energy ($E=6.547$ keV). Lower: Scan along $(0,k,0)$ for the $x=0.4$ sample at $T=30$ K ($E=8$ keV).

$$I^{\mathrm{res}}_{\sigma\to\pi'}(\psi)=\frac{A^4\Delta^2\sin^2\psi}{[\Gamma^2+4(2\Delta-x)^2][\Gamma^2+4(\Delta+x)^2]}, \qquad (2)$$

where $x=(\omega-\omega_0)$. This simple model thus predicts that the scattering is all of the $\sigma\to\pi$ type and that it has a twofold azimuthal symmetry, with zeros coming when the incident polarization is parallel to the *c* axis. The azimuthal angle characterizes rotations of the sample about the scattering wavevector, and is defined to be zero when the *c* axis is perpendicular to the scattering plane (Fig. 4). Although a detailed analysis of the data requires a more sophisticated treatment, this model captures many of the essential elements of the experimental results, as will be shown below.

It is worth adding that there should also be nonresonant scattering from an orbitally ordered material. However, for the structures shown in Fig. 3, and the $(0,k,0)$ reflections, the charge density is arranged symmetrically, and the scattering is zero. It is nevertheless still possible that nonresonant charge scattering can arise at the orbital wavevector from lattice modulations accompanying the orbital ordering, and such a modulation has been observed in $Pr_{1-x}Ca_xMnO_3$ (see, e.g., Refs. 5, 43, and 44) and in $La_{0.5}Ca_{0.5}MnO_3$.[6,29–31] In fact, one result of the present work is the observation of a longitudinal component of this modulation for the $x=0.4$ and 0.5 samples, which we will also discuss below.

V. RESULTS

A. Diffraction pattern

Scans of the resonant scattering intensity versus momentum transfer along the $(0,k,0)$ direction are shown for the $x=0.25$ and $x=0.4$ samples, respectively, in Figs. 5(a) and 5(b). Results for the $x=0.5$ sample are similar to those shown for $x=0.4$, and are not shown. In each case, the samples were cooled below their ordering temperatures, to $T=300$ K and $T=30$ K for the $x=0.25$ and the $x=0.4$

samples, respectively. The intensities are plotted versus k in counts per second and shown on a logarithmic scale. Twinning within the ab plane was observed in all three samples. It is visible as a peak splitting in low-momentum-transfer resolution scans, such as shown in Fig. 5(a) for the $x=0.25$ sample. This splitting is not observed in high-resolution scans, for which the resolution volume never overlaps the second peak [Fig. 5(b)].

The large peaks falling at $k=2,4$ in both scans in Fig. 5 correspond to bulk allowed Bragg reflections expressed in orthorhombic units. Their intensities were obtained using Al absorbers, and should be considered qualitative. Referring to the $x=0.25$ sample [Fig. 5(a)], the peaks at $k=1,3$ correspond to orbital ordering with the periodicity defined in Fig. 3(a). Count rates of 400/sec were obtained at the (0,1,0) reflection on the NSLS X21 wiggler beam line. For the $x=0.4$ sample, the peaks at $k=0.5$, 1.5, and 2.5 correspond to orbital ordering, while those at $k=1,3$ correspond to charge ordering, both with the periodicities defined in Fig. 3(b). Typical count rates for this sample obtained at the NSLS bending magnet beam line X22C reached 1500/sec at the (010) reflection and 3000/sec at the (0,1.5,0) reflection. Considering the many differences between the two beam lines and the geometries employed, we have not attempted to make quantitative comparisons of the intensities. The origins of the peaks at $k\approx0.65$ and 1.4 are unknown. Both peaks persisted in the diffraction pattern above the charge- and orbital-ordering temperatures, however, and were not studied further.

It is clear from the figure that the wavevectors for charge and orbital ordering in all three samples are simply commensurate with the lattice, and independent of concentration. Further, the measured peak positions are all consistent with the periodicities proposed in Fig. 3 for the different orbital and charge ordered structures. The temperature dependence of the charge and orbital order wavevectors will be discussed further in Sec. V C below.

B. Resonant scattering

1. Orbital reflections

Figure 6 shows the energy dependence of the scattering at the (100) orbital wavevector of the $x=0.25$ sample as the incident x-ray energy is tuned through the Mn K absorption edge (6.539 keV). These data were obtained with a Si(111) analyzer on the CMC-CAT undulator beam line 9ID at the Advanced Photon Source (APS). A large resonant signal is visible at $\hbar\omega=6.547$ keV, reaching more than 20 000 counts per second near the edge. In addition, there are two smaller peaks at higher energies ($\hbar\omega=6.56$ and 6.575 keV), and one below (at $\hbar\omega=6.534$ keV). The inset shows the lower-energy peak in more detail. No signal was observed at energies 100 eV above or below the absorption edge, implying that only pure resonant scattering was present in this sample. Polarization analysis (performed on bending magnet beam line X22C at the NSLS) suggests that the scattered signal is predominantly π polarized, consistent with a rotation of the incident linear polarization from being perpendicular to the diffraction plane, σ, to lying within the diffraction plane, π. It should be added that all of the data shown here, and in Figs. 7, 10, and 11 below, were obtained at an azimuthal angle $\psi=90°$. As a function of azimuthal angle, the resonant intensity observed for the $x=0.25$ sample takes maxima at $\psi=90°$ and 270°, and minima at 0° and 180°. All these results are all similar to those obtained previously at the orbital wavevector of $LaMnO_3$, including the four-peaked fine structure in the energy dependence, an identical polarization and azimuthal dependence, and the absence of nonresonant scattering away from the edge.[7,45]

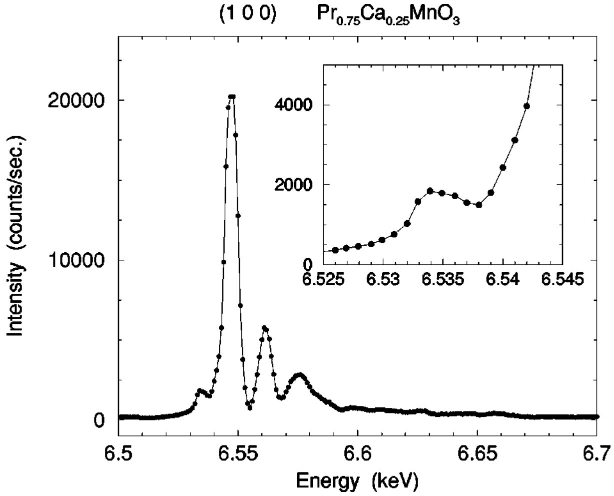

FIG. 6. Intensity plotted versus incident photon energy of the orbital (010) reflection of the $x=0.25$ sample near the Mn white line at 6.547 keV. These data were taken at APS beam line 9ID with an energy resolution of 1.5 eV. Inset: Closeup of the preedge feature at 6.535 keV.

Figures 7(a) and 7(b) show the energy dependence of the scattering at the (0,1.5,0) and (0,2.5,0) orbital wavevectors of the $x=0.4$ sample, again as the incident x-ray energy is tuned through the Mn K absorption edge. These data were

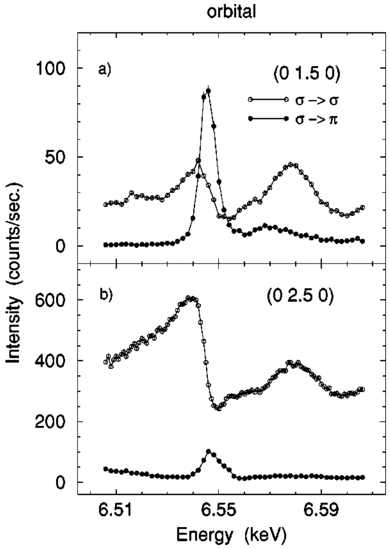

FIG. 7. Polarization-resolved scans of intensity plotted versus incident photon energy of the orbital (0,1.5,0) and (0,2.5,0) reflections of the $x=0.4$ sample near the Mn K absorption edge.

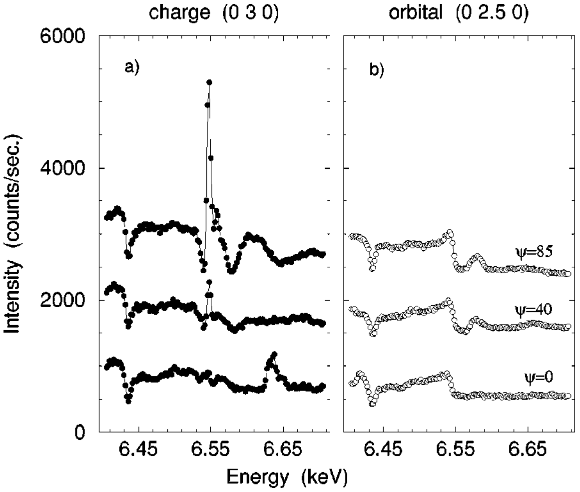

FIG. 8. Intensity plotted versus incident photon energy of the charge (0,3,0) and orbital (0,2.5,0) reflections of the $x=0.4$ sample for three different values of the azimuthal angle. The feature at $E=6.62$ keV and $\psi=0$ in the charge order scattering is attributed to multiple scattering.

obtained on the X22C bending magnet beam line at the NSLS, and explicitly resolve the polarization. The closed circles show the $\sigma\rightarrow\pi$ scattering, and the open circles show the $\sigma\rightarrow\sigma$ scattering. Although the fine structure in Fig. 7(a) is not as clearly resolved as in the $x=0.25$ sample, the main features of the $\sigma\rightarrow\pi$ scattering are similar, including a pronounced resonance peak at 6.547 keV and a weaker peak at 6.57 keV. In contrast to the $\sigma\rightarrow\pi$ scattering, the $\sigma\rightarrow\sigma$ scattering shows a double-peaked structure with a pronounced dip at the absorption edge. This is strongly reminiscent of the behavior of charge scattering, and suggests the presence of a lattice modulation with the orbital wavevector. The fact that the $\sigma\rightarrow\sigma$ intensity does not fall off at lower x-ray energy, but instead continues above background, is further evidence of a significant nonresonant signal as would be produced by such a modulation. Lattice modulations associated with the CE-type structure have been observed before in $Pr_{1-x}Ca_xMnO_3$, e.g., Refs. 5, 27, 43, and 44, and also in $La_{0.5}Ca_{0.5}MnO_3$.[6,21,23] In the latter compound, the structure was solved, and the modulation found to be purely transverse. Such a modulation, however, is inconsistent with the present results. We will return to this point below.

A broader-ranged energy scan of the (0,2.5,0) orbital wavevector is shown for the $x=0.4$ sample in Fig. 8. These data were taken with a Ge(111) analyzer, and are plotted versus energy for several different azimuthal angles. The use of a Ge analyzer implies that both $\sigma\rightarrow\sigma$ and $\sigma\rightarrow\pi$ components are detected, and that their intensities add. Referring to the scan for $\psi=85°$, the basic features shown in Fig. 7(b) are reproduced, although the $\sigma\rightarrow\sigma$ scattering clearly dominates the signal. Below the Mn absorption edge, the observed scattering is approximately constant until it reaches the Pr L_2 absorption edge energy at 6.43 keV. There the intensity again shows a dip, primarily as a result of the increase in the absorption. Qualitatively similar results were obtained for the $x=0.5$ sample.

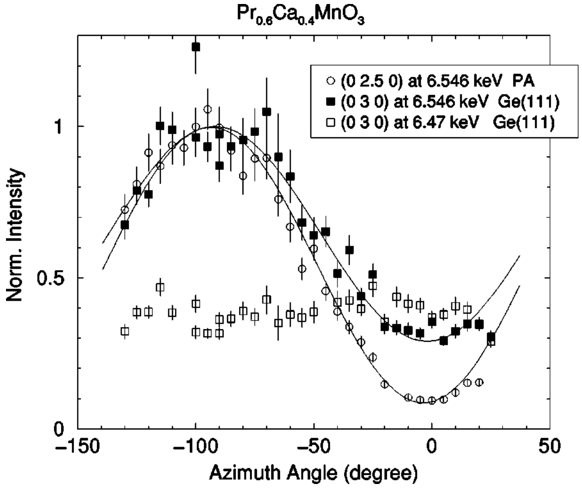

FIG. 9. Azimuthal dependence of the charge and orbital ordering intensities both on and off the Mn K-edge resonance, as obtained for the $x=0.4$ sample.

It is clear from Fig. 8 that except for a variation of the overall intensity, no new features are introduced as a function of azimuthal angle. A quantitative study of the azimuthal dependence of the orbital scattering at (0,2.5,0) is shown in Fig. 9, in which the maximum resonant intensity in the $\sigma\rightarrow\pi$ geometry was recorded versus azimuthal angle for rotations over 180° (open circles). The data have been normalized by the average intensity of the (0,2,0) and (0,4,0) fundamental Bragg reflections to correct for small variations due to sample shape. Again, $\psi=0$ corresponds to a configuration in which the c axis is perpendicular to the diffraction plane. In contrast to a normal charge reflection, for which the intensity is independent of the azimuthal angle, the resonant scattering exhibits a characteristic oscillation with a twofold symmetry. The intensity approaches zero when $\psi=0°$ and 180°, consistent with the $\sigma\rightarrow\pi$ polarized component of the resonant scattering in the $x=0.25$ sample. The solid line in Fig. 9 is a fit to the form $A\sin^2\psi$, as predicted in Eq. (2).

To summarize: In all three samples, we find a pure resonant signal in the $\sigma\rightarrow\pi$ channel at the appropriate orbital wavevector with the dominant peak located near the Mn K absorption edge. Additional fine structure is observed both above and below the absorption edge. The π-resonant scattering has the characteristic azimuthal dependence, varying as $\sin^2\psi$, where ψ is the azimuthal angle. These results are identical to what has been observed previously in $LaMnO_3$ (Ref. 8) and $La_{0.5}Sr_{1.5}MnO_4$.[7] In the $x=0.4$ and 0.5 samples, there is in addition a $\sigma\rightarrow\sigma$ component of the scattering at the orbital wavevector with both resonant and nonresonant parts. The nonresonant component lacks any azimuthal dependence and is consistent with normal charge (or Thomson) scattering. The $x=0.25$ sample lacks a $\sigma\rightarrow\sigma$ component to within the detection limits of the experiment, as was also the case in $LaMnO_3$.

We associate the dominant, resonant peak, which occurs in the $\sigma\rightarrow\pi$ channel of all three samples with the electric dipole transition coupling $1s$ and $4p$ states, as discussed in Sec. IV. Recall that the sensitivity to orbital ordering may be thought of, qualitatively, as arising from a splitting of the Mn $3d$ states, either through the Jahn-Teller distortion of the oxygen atoms or through a Coulomb interaction. In either case, the existence of a dipole resonance in the $\sigma \rightarrow \pi$ channel, and the observed azimuthal dependence, are consistent with theoretical predictions. We therefore interpret the observed resonant scattering as Templeton scattering induced by the orbital ordering, just as previously concluded for $LaMnO_3$ and $La_{0.5}Sr_{1.5}MnO_4$.[7,8] To explain the additional fine structure both above and below the main peak, however, requires a more sophisticated treatment. Elfimov *et al.*,[11] in particular, have performed band-structure calculations for $LaMnO_3$ with a LSDA+U-type approach, and shown that the fine structure above the absorption edge reflects the $4p$ density of states after hybridization of the central Mn $4p$ and surrounding O $2p$ states. They show further that the higher-energy peaks originate predominantly from the Jahn-Teller distortion of the oxygens, and not from direct Coulomb interactions. In contrast, the small peak about 13 eV below the white line is associated with the intersite $4p$-$3d$ hybridization of the central and neighboring Mn ions via the intervening O $2p$ states. Although quantitative comparisons remain to be made, the qualitative agreement between these predictions and the observed spectra is good, and offers a natural description of the experimental results. In this regard, it should be added that Ishihara and Maekawa[46] have also carried out cluster calculations of the resonant cross section in $LaSr_2Mn_2O_7$, assuming an intrasite $3d$-$4p$ Coulomb origin of the $4p$ splitting. By including band effects, they also were able to produce a qualitatively similar fine structure above the Mn K edge. Thus, we are not able to distinguish a possible Coulomb origin of the resonant peak from a Jahn-Teller origin on the basis of our experiments—however, the additional fine structure at higher photon energies appears to result from band effects in both approaches.

It is worth noting that the energy of the preedge feature (see inset, Fig. 6) corresponds to that of the Mn $3d$ states. Several groups have shown that this feature is highly sensitive to the $3d$ orbital occupancy,[11,24,10,47] but not to the Jahn-Teller distortion (oxygen motion)—in contrast with the main-edge feature. In fact, states of both d- and p-like symmetry (with respect to the central ion) exist at the preedge energy, with significantly more weight in the d-like states,[47] suggesting that both dipole and quadrupole processes should contribute. Takahashi *et al.* estimate that the total intensity, enhanced by interference with the main-edge processes, is about 1% of the main edge. In our experiment, we find that the preedge intensity is about 5% of the main-edge intensity. However, the absorption correction has not been included. The latter would reduce the intensity ratio towards 1%. In addition, Takahashi *et al.*[47] predict two distinct features in the energy dependence of the scattering separated by 3 eV. In contrast, we observe only a single feature using an energy resolution of 1.5 eV. In principle, the preedge feature could exhibit different azimuthal[47] and temperature dependences from those of the main-edge feature. In our studies of the azimuthal and temperature dependence however, we found no difference between the preedge and main-edge behaviors, to within errors.

We note, in passing, that in V_2O_3 the resonant ion is not in a center of inversion symmetry and that, therefore, dipole transitions are allowed directly into the d band of that material. This gives rise to a large preedge feature that has also been used to study orbital order[10,16] by resonant x-ray scattering techniques.

We now turn to the lattice modulation observed at the orbital wavevector in the $\sigma \rightarrow \sigma$ channel. Such modulations have been observed before in CE-type structures, and in particular in $Pr_{1-x}Ca_xMnO_3$ by neutron[3,5,27,44] and nonresonant x-ray scattering.[44,48] Similar results have also been obtained in $La_{0.5}Ca_{0.5}MnO_3$ (Ref. 6) at $(h,k/2-\epsilon,2n)$, where $h \neq 0$ and ϵ, the incommensurability, is weak (we have converted to $Pbnm$ settings to be consistent with the present paper). The latter structure was solved by x-ray powder diffraction and a purely transverse modulation of the Mn^{4+} sites was deduced, wherein the Mn^{4+} sites are displaced along the a direction with a periodicity equal to the orbital periodicity. All of the orbital superlattice peaks observed to date in the $Pr_{1-x}Ca_xMnO_3$ system have also had a significant a-axis component and a similar distortion has been assumed.[5,27]

In the present case, the $\sigma \rightarrow \sigma$ scattering observed at $(0,k+\frac{1}{2},0)$ requires a longitudinal b-axis component of the modulation. This follows from the small-displacement limit of the x-ray intensity, which varies as $|\vec{Q}\cdot\vec{\delta}|^2$ to leading order for displacements of the form $\vec{\delta}\sin(\vec{\tau}\cdot\vec{R})$. Recently, we have performed scans of the (2,1/2,0) reflection of the $x=0.4$ sample, and found significant nonresonant scattering at 200 K [$\sim$10 000/sec with a Si(111) analyzer]. This is consistent with a large transverse displacement and a small longitudinal modulation. Similar results have also been found in our recent studies of an $x=0.3$ sample.[49] We will return to the subject of this lattice modulation again shortly.

It is also worth commenting on the differences between the $La_{0.5}Ca_{0.5}MnO_3$ structure and the present case. In $La_{0.5}Ca_{0.5}MnO_3$, a temperature-dependent incommensurability was observed at the orbital wavevector,[6,26] whereas in the present case the scattering appears strictly commensurate. The source of the incommensurability in the former material is believed to be an ordered array of domain walls—discommensurations—separating regions of commensurate order. As is discussed below, we observe domain walls at a similar spacing in $Pr_{0.5}Ca_{0.5}MnO_3$. Thus, the main difference between the two structures appears to be that the domain walls are ordered in $La_{0.5}Ca_{0.5}MnO_3$, but disordered in $Pr_{1-x}Ca_xMnO_3$. It is an interesting question as to why this is so.

2. Charge-order reflections

Figures 10(a) and 10(b) show the energy dependence of the scattering at the (0,1,0) and (0,3,0) charge-order wavevectors of the $x=0.4$ sample, as the incident x-ray energy is tuned through the Mn K absorption edge. These data were obtained at the NSLS beam line X22C and are polarization resolved. The open circles show the $\sigma \rightarrow \sigma$ scattering and the closed circles the $\sigma \rightarrow \pi$ scattering. No signal was obtained in the $\sigma \rightarrow \pi$ channel, to within the detection limits of the experiment. In the $\sigma \rightarrow \sigma$ channel, the (0,1,0) reflection

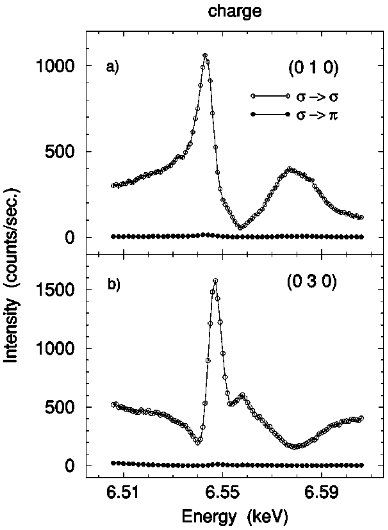

FIG. 10. Polarization-resolved scans of the intensity plotted versus incident photon energy of the charge (0,1,0) and (0,3,0) reflections of the $x=0.4$ sample near the Mn K absorption edge.

has a shoulder at lower energy that rises to a resonant peak at 6.544 keV. This is followed by a dip and another smaller peak centered near 6.58 keV. The profile of the (0,3,0) reflection shows a resonant peak at slightly higher energy (6.546 keV) relative to the (0,1,0) reflection, and the additional structure appears inverted. This is a clear signature of an interference process, involving the resonant and nonresonant contributions to the charge order scattering. The nonresonant scattering may, in principle, result from the valence modulation itself (which is weak), or from an accompanying lattice modulation, or both. The resonant scattering arises from the anomalous parts of the Mn^{3+} and Mn^{4+} scattering factors, which are distinct.

For comparison, the energy dependence of the scattering at the charge order wavevector (010) of the $x=0.5$ sample is shown in Fig. 11. The data were obtained without an analyzer, and so include both the $\sigma\rightarrow\sigma$ component and any $\sigma\rightarrow\pi$ component. The line shape is nearly identical to that obtained for the $x=0.4$ sample at the same reflection.

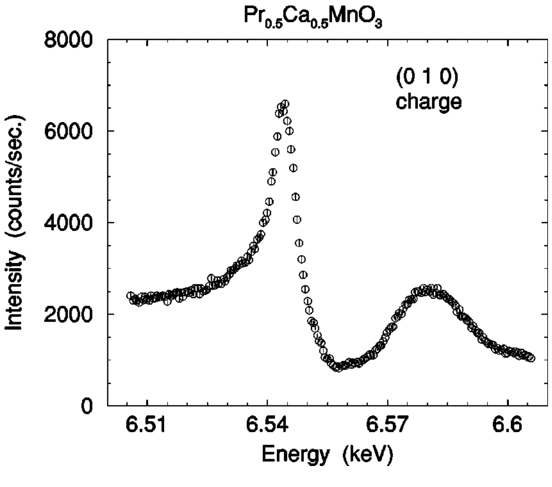

FIG. 11. Intensity plotted versus incident photon energy of the charge (0,1,0) reflection of the $x=0.5$ sample, near the Mn K absorption edge.

A series of broader ranged energy scans of the (0,3,0) reflection taken at various azimuthal angles for the $x=0.4$ sample is shown in Fig. 8. The basic features noted in Fig. 10 are reproduced there. In addition, there is a dip in the scattering at 6.44 keV, which reflects the Pr L_2 absorption edge. We believe that the peak at 6.64 keV in the scan at $\psi=0$ arises from multiple scattering and can be ignored. Except for a decrease of the resonant intensities, very little else changes in these spectra as a function of azimuthal angle, as was also observed for the orbital-ordering reflection.

A quantitative study of the dependence of the charge-order scattering on the azimuthal angle, at the (0,3,0) reflection is shown in Fig. 9. The filled squares record the behavior of the maximum resonant intensity obtained at 6.546 keV, while the open squares give the intensity measured off resonance at 6.47 keV. As before, these data have been normalized by the average of the (020) and (040) fundamental Bragg intensities. In contrast to the nonresonant charge-order scattering, which is flat as expected, the resonant charge-order scattering exhibits a pronounced azimuthal dependence, with the same sine-squared behavior as observed above for the resonant orbital scattering.

A possible explanation of the azimuthal dependence follows simply from the Mn contribution to the structure factor of $(0,k,0)$ charge-type peaks:

$$f(0,k=\mathrm{odd},0)=f_{3+}^{n=1}+f_{3+}^{n=-1}-2f_{4+}. \tag{3}$$

$f_{3+}^{n=1(n=-1)}$ are the atomic form factors for the Mn^{3+} ions on the two orbital sublattices, where $n=1,-1$ is defined in Fig. 4. As emphasized above, these quantities are second rank tensors near resonance. We take f_{4+} to be spherically symmetric and write

$$f_{3+}^{n=-1}=\begin{pmatrix} a & 0 & 0\\ 0 & b & 0\\ 0 & 0 & b \end{pmatrix},\quad f_{3+}^{n=1}=\begin{pmatrix} b & 0 & 0\\ 0 & a & 0\\ 0 & 0 & b \end{pmatrix}, \tag{4}$$

where $f_{3+}^{n=-1}$ and $f_{3+}^{n=1}$ have the symmetries $3x^2-r^2$ and $3y^2-r^2$, respectively. Calculating the polarization and azimuthal dependence of the scattering,

$$I=|\vec{\epsilon}_i\cdot\tilde{F}_{0k0}(\psi)\cdot\vec{\epsilon}_f|^2, \tag{5}$$

we find a twofold azimuthal dependence in the $\sigma\rightarrow\sigma$ channel, with zeros at $\psi=0$ and 180°, as observed. In addition, Eq. (5) predicts a $\sigma\rightarrow\pi$ component with a fourfold symmetry (with zeros at 0°, 90°, 180°, 270°) although with a significantly smaller intensity (which we were unable to observe). We remark that it is the anisotropy of the structure factor $f(0,k=\mathrm{odd},0)$ that gives rise to the observed azimuthal dependence. In this sense, the ‘‘charge-order’’ reflection has some orbital character.

In order to model the energy dependence of the charge-order scattering, we write the structure factor as a sum of the scattering factors of the Mn^{3+} and Mn^{4+} ions within the unit cell, including both resonant and nonresonant terms for each.[50] Here, for simplicity, we neglect the tensor character discussed above, and treat the form factors as (complex) scalars. Figure 12(a) shows schematic forms of the real and imaginary parts of the Mn^{3+} scattering factor, plotted versus incident photon energy. As our intention in the following was simply to gain a qualitative understanding of the energy line shape we have chosen functional forms for the real and imaginary parts of the Mn scattering factor that model the energy dependence in a generic way. Thus, the imaginary part approximates a step function and the real part contains a dip at the edge. Oscillations were added to both components above the edge. These forms [Fig. 12(a)] resemble experimental results (see, for example, Ref. 51) but are not intended to correspond to the actual properties of Mn. None of the conclusions drawn from this model depend on the details of the functional forms used. The Mn^{4+} scattering factor was obtained from that of Mn^{3+} by shifting the curve by 4 eV, following Murakami *et al.*[7] (see also Ref. 52). Assuming that the Mn displacements δ are along the b axis with modulation wavevector $(0,k,0)$ in the $x=0.4$ and 0.5 samples, the structure factor for the scattering from the Mn may be written:

$$f(0,k=\mathrm{odd},0)=f_{3+}e^{i\pi k\delta}-f_{4+}e^{-i\pi k\delta}, \tag{6}$$

where δ is a displacement parameter (in units of b, the lattice constant). This reduces to the simple form $(f_{3+}-f_{4+})$ when $\delta=0$, as expected. In addition, a constant term representing the longitudinal oxygen motion has been included.

Plots of the energy dependence of the intensity predicted by this model for $\delta=0$ and including the nonresonant scattering arising from oxygen motion are shown in Fig. 12(b) for the (0,1,0) and (0,3,0) reflections. They reproduce the basic features of the line shapes in Fig. 10, including the interference and the phase shift observed in the oscillations observed above the edge. The line shapes also resemble those generated by Murakami *et al.*[7] for $\mathrm{La}_{0.5}\mathrm{Sr}_{1.5}\mathrm{MnO}_4$, using a more quantitative model. If the manganese atoms are then allowed to move $(\delta\neq 0)$, the small shift of the peak maximum of the (0,1,0) reflection relative to the (0,3,0) reflection is also described, as illustrated in Fig. 12(c).

We emphasize that although this model captures qualitative features of the line shape of the charge-order scattering, a quantitative analysis is required before it can be considered as definitive. We note in this regard that there are other points of view. In particular, x-ray absorption near-edge spectroscopy (XANES) measurements of $\mathrm{La}_{1-x}\mathrm{Ca}_x\mathrm{MnO}_3$ by Booth *et al.*[52] have been interpreted in terms of a mixed valence description of the electronic structure, explicitly ruling out the Mn charge modulation assumed here. In such a scenario, our experimental results imply the existence of two Mn sites that are distinguishable by the anisotropy of their environments, but not by their valence. Our results further imply that this anisotropy is ordered, which leads to resonant, structural harmonics at the charge and orbital wavevectors. Such a model correctly describes the polarization and azimuthal dependence of the resonant scattering, but must still explain its temperature dependence, including the variation of the peak widths above and below the charge- and orbital-ordering temperature (described below), and the dif-

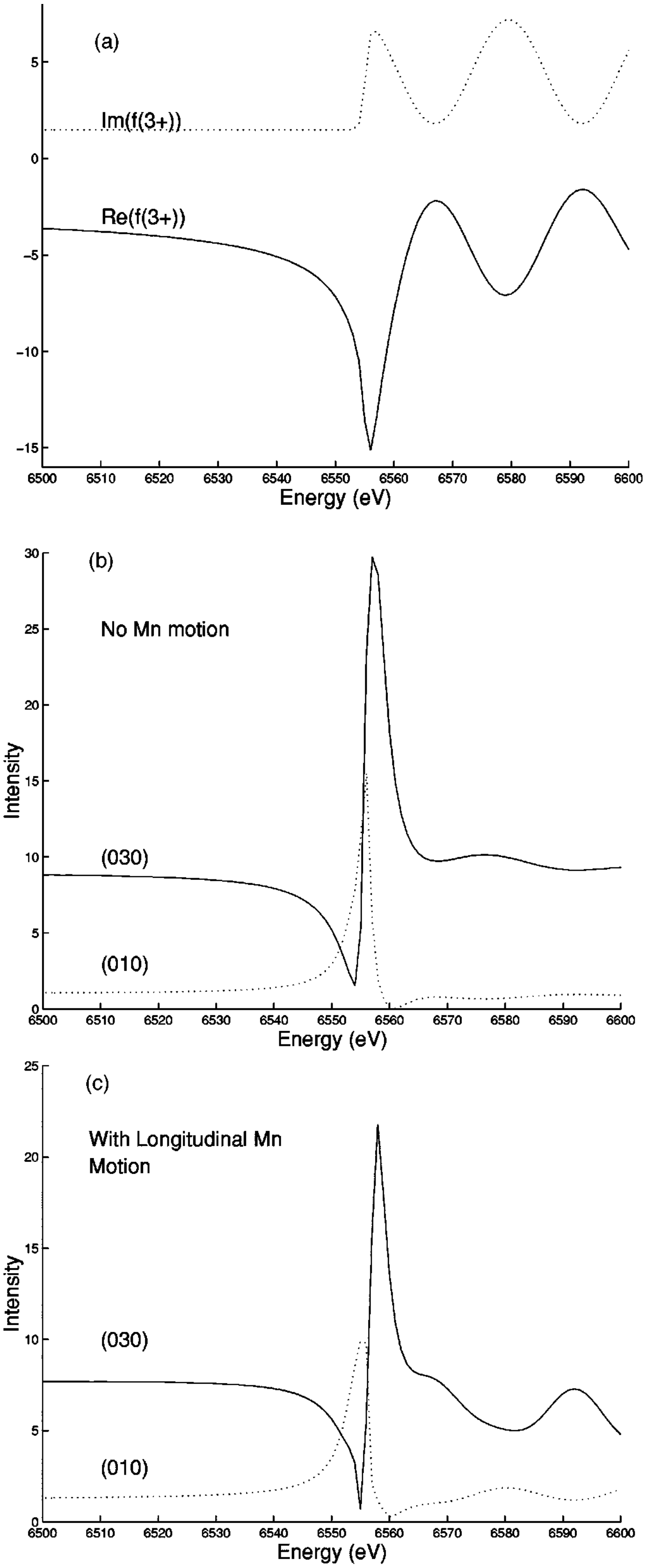

FIG. 12. (a) Real and imaginary parts of a generic scattering factor for Mn^{3+} plotted near the K edge. These are shifted by 4 eV to obtain the corresponding scattering factor for Mn^{4+}. (b) Intensity plotted versus incident photon energy including a longitudinal distortion of the oxygen positions and using the scattering factors shown in (a). (c) Same as in (b), but with the addition of a longitudinal Mn displacement.

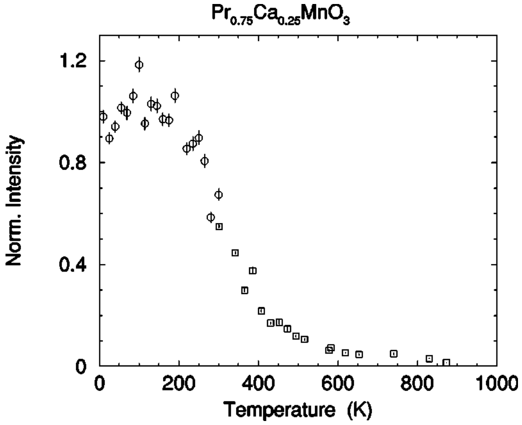

FIG. 13. Temperature dependence of the scattering at the orbital (0,3,0) reflection of the $x=0.25$ sample. Open circles represent data taken on beam line X22C, open squares taken at beam line X21. The data sets have been scaled to agree at room temperature.

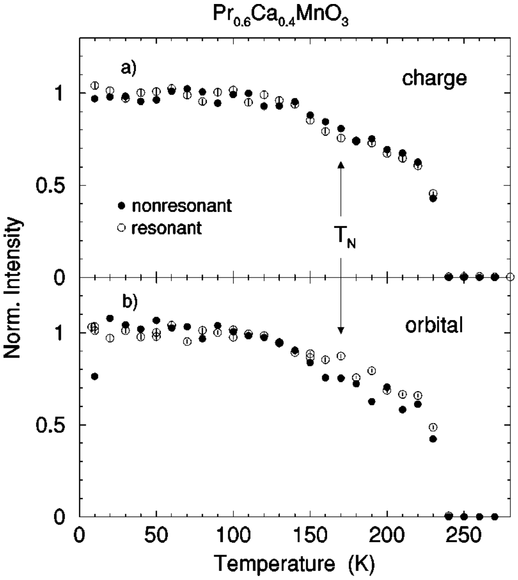

FIG. 14. Upper: Temperature dependence of the scattering at the charge (0,3,0) reflection of the $x=0.4$ sample. Open circles were obtained on resonance and closed circles off resonance. Lower: Temperature dependence of the scattering at the orbital (0,1.5,0) and (0,2.5,0) reflections of the $x=0.4$ sample. The data at the (0,1.5,0) reflection (open circles) were obtained on resonance at the Mn K edge, while those at the (0,2.5,0) reflection (closed circles) were obtained off-resonance. Note that resonant scattering at the (0,1.5,0) reflection is dominated by the orbital $\sigma\rightarrow\pi$ contribution in Fig. 7, and not that of the lattice modulation.

ference in the k odd-integer and half-integer order reflections. It must also account for the existence of lattice modulations at the charge and orbital wavevectors, as well as for the complex, and temperature-dependent, magnetic structures.

It is finally worth noting that a simple transverse displacement cannot explain the nonresonant x-ray results for the charge ordering, just as was noted earlier for the modulation accompanying the orbital ordering. On the basis of these results, we conclude that the $x=0.4$ and 0.5 samples exhibit lattice modulations with displacements along the b direction, and produce scattering at both the charge and orbital wavevectors. A fuller understanding of the lattice distortions observed in these materials will require further experiments.

C. Temperature dependence

1. Intensities

The temperature dependence of the orbital-ordering intensity between 10 and ≈850 K is shown for the $x=0.25$ sample in Fig. 13. Each point represents the peak intensity obtained from a k scan of the (0,1,0) reflection, such as is shown in Fig. 5(a). Circles and squares represent the results of two different runs, one taken at high temperatures with the sample heated in an oven and the other at low temperatures with the sample cooled in a cryostat. The two data sets were then scaled to be equal at 300 K. Referring to Fig. 13, the orbital intensity is approximately constant (to within 3σ) between 10 and 200 K, and decreases gradually with a long tail until about 850 K—a surprising result. High-momentum-transfer resolution scans showed further that the orbital peak widths were independent of temperature and resolution-limited throughout the ordered phase. Thus, the intensities shown in Fig. 13 may be regarded as integrated intensities. The resolution-limited behavior also implies that the corresponding orbital correlation lengths were at least 2000 Å along the b direction.

The temperature dependences of the integrated charge- and orbital-ordering intensities of the $x=0.4$ sample are plotted between 10 and 300 K in Figs. 14(a) and 14(b). The charge-order intensities were obtained at the (0,3,0) reflection both at resonance using a Ge(111) analyzer and off-resonance at 6.6 keV. The latter employed a Cu(220) analyzer. The orbital intensities were obtained at resonance at the (0,1.5,0) reflection, where the resonant $\sigma\rightarrow\pi$ scattering dominates the signal and off-resonance at the (0,2.5,0) reflection, with an incident photon energy of 6.47 keV. Both data sets for the orbital ordering were obtained using a Ge(111) analyzer.

Referring to the figure, the orbital and charge intensities are approximately constant between 10 and 130 K, but begin to decrease above ≈130 K. They drop abruptly at 245 K, consistent with a first-order, or nearly-first-order, transition. It is clear from the figure that the temperature dependences of the resonant and nonresonant intensities are identical for the charge and orbital ordering, respectively, at least to within the present counting statistics. This suggests that the lattice modulation accompanying the charge and orbital ordering reflects the same order parameter. The temperature dependences of the charge and orbital ordering in the $x=0.4$ sample are also very similar, as shown directly in an earlier publication.[15] There we speculated that the charge and orbital ordering might be linearly coupled. More recently, Zhang and Wang have argued on the basis of a Landau theory that the charge and orbital ordering in $Pr_{1-x}Ca_xMnO_3$ are quadratically coupled,[28] but that the coupling is sufficiently strong that they have very similar temperature dependences over the range considered here.

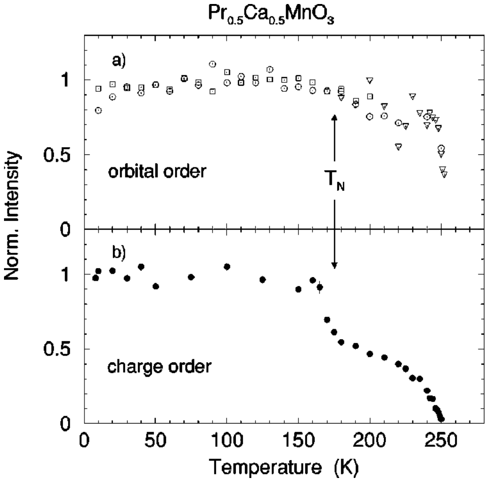

FIG. 15. Upper: Temperature dependence of the scattering at the orbital (0,1.5,0) reflection of the $x=0.5$ sample. Circles and squares were obtained with a Ge(111) analyzer, triangles with a Cu(220) analyzer. Lower: Temperature dependence of the scattering at the charge (0,1,0) reflection obtained with a Ge(111) analyzer.

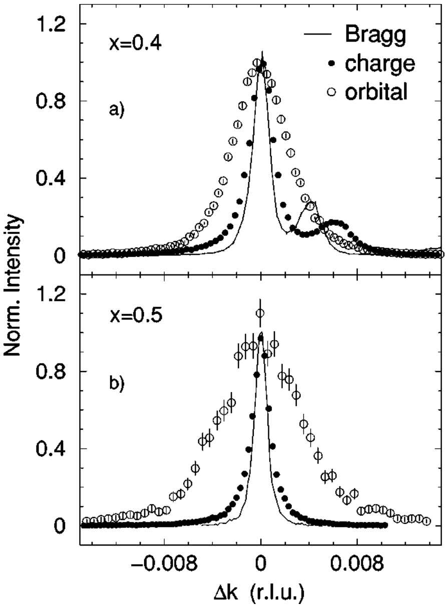

FIG. 16. Upper: Longitudinal scans of the Bragg (0,2,0), the charge (0,1,0), and the orbital (0,2.5,0) reflections of the $x=0.4$ sample at $T=8$ K. Lower: The same for the $x=0.5$ sample. Data have been normalized to the same peak intensity to facilitate comparison.

The temperature dependences of the orbital- and charge-order intensities of the $x=0.5$ sample between 10 and 300 K are shown in Figs. 15(a) and 15(b). The orbital ordering intensities were again obtained from k scans of the (0,1.5,0) reflection using Ge(111) and Cu(220) analyzer configurations, with the latter in a $\sigma \rightarrow \pi$ geometry. The signal rates in these experiments were weak (<10/sec at $T=220$ K), making a definitive characterization of the temperature dependence difficult. Charge-order intensities were obtained at the (0,1,0) reflection using a Ge(111) analyzer. All of these data were obtained at the Mn K-edge resonance.

Referring to Figs. 15(a) and 15(b), the orbital-ordering intensity is approximately constant between 10 and 150 K, and begins to fall off between 150 and 200 K, reaching zero at about 250 K. The charge-order intensity is also constant between 10 and 150 K, but exhibits a much clearer decrease near the Néel temperature $T_N=170$ K. A similar decrease at T_N was observed for the orbital intensity of $LaMnO_3$,[8] where a correlation was made between the long-range antiferromagnetic order and the orbital order. Although this trend is suggested in each of the samples studied here, with $T_N=140$, 170 and 180 K in the $x=0.25$, 0.4, and 0.5 samples, respectively, only the data for the charge ordering of the $x=0.5$ sample is convincing. Despite repeated attempts to quantify this behavior in the other samples, we still cannot claim to have measured a definitive link between the magnetic ordering and the charge and orbital ordering in each case.

2. Correlation lengths

High-momentum-transfer-resolution longitudinal scans of the Bragg, charge-, and orbital-ordering line shapes of the $x=0.4$ and 0.5 samples are superimposed on each other for comparison in Figs. 16(a) and 16(b). The data were obtained at low temperatures (10 K) in the ordered phase using a Ge(111) analyzer. Solid lines indicate the results of scans through the (0,2,0) Bragg peaks; open circles indicate scans through (0,2.5,0) orbital peaks; and filled circles give the results obtained for the (0,3,0) and (0,1,0) reflections of the charge-ordered peaks of the $x=0.4$ and 0.5 samples, respectively. It is clear from the figure that the Bragg and charge-order peaks have similar widths, approximately corresponding to the momentum-transfer resolution at each Q. This implies that the correlation lengths of the structure and of the charge order are at least 2000 Å in each case. The small differences in width probably reflect the Q dependence of the resolution function. In contrast, the orbital-ordering peaks in both samples are significantly broader than the resolution, implying smaller orbital domain sizes.

Estimating the correlation length, ξ, with $\xi=b/2\pi\Delta k$, where b is the lattice constant, and Δk the half-width of the orbital peaks, we find orbital correlation lengths $\xi=320\pm10$ Å and 160 ± 10 Å for the x = 0.4 and 0.5 samples, respectively. We note that in the analysis the charge-order peaks were fitted with Lorentzian line shapes, while the orbital-ordering peaks were fitted with squared Lorentzians. When necessary for deconvolution, a Lorentzian-squared resolution function was used, as derived from the structural Bragg peaks. These line shapes were chosen simply for the quality of the fit, and have not been justified theoretically.

It follows from these correlation lengths that the $x=0.4$ and 0.5 samples do not exhibit long-range orbital order, but instead form a domain state with randomly distributed antiphase domain boundaries. A schematic view of such a domain wall is shown in Fig. 3(c). In contrast, the charge ordering is much more highly correlated.

The presence of an orbital domain state sheds light on recent neutron diffraction studies of $Pr_{0.5}Ca_{0.5}MnO_3$ (Refs. 53 and 27) and powdered $La_{0.5}Ca_{0.5}MnO_3$ (Ref. 29). In the

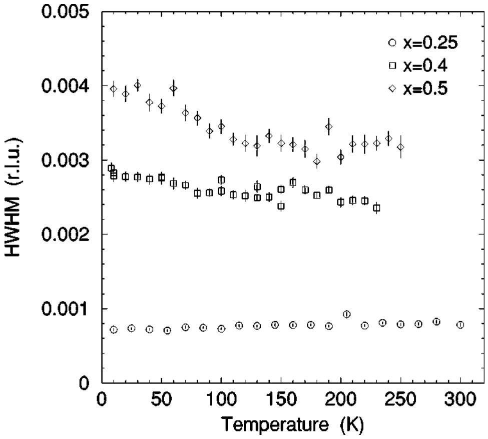

FIG. 17. Temperature dependence of the half widths at half maximum of the orbital (0,1,0) reflection of the $x=0.25$ (diamonds), $x=0.4$ (0,1.5,0) (squares), and $x=0.5$ reflection (circles) samples. Note: These widths represent the raw data, i.e., without corrections for resolution effects.

former it was shown that the magnetic correlation length was finite. In $La_{0.5}Ca_{0.5}MnO_3$, which also exhibits the CE magnetic structure with orbital and charge order,[6] separate magnetic correlation lengths were extracted for the Mn^{3+} and Mn^{4+} magnetic sublattices, with the remarkable result that they were quite different: $\xi_{3+}^{\mathrm{mag}}=250-450$ Å and $\xi_{4+}^{\mathrm{mag}} \geqslant 2000$ Å, respectively. Those authors proposed antiphase domain walls composed of "misoriented" e_g orbitals to explain the magnetic disorder of the Mn^{3+} sublattice. Such domain walls break the magnetic coherence on the 3+ sublattice only, as long as the charge order is preserved [Fig. 3(c)]. Our results strongly suggest that this interpretation is correct, and that we have observed these antiphase domains directly in the orbital reflection (although in a different material). These results taken together suggest that such orbital domain states are common to these systems—at least in this range of doping. Note that these domains are believed to be static, and do not correspond to the (dynamic) orbital fluctuations inferred from magnetic neutron diffraction investigations of the ferromagnetic spin fluctuations in $Pr_{1-x}Ca_xMnO_3$, which disappear below T_N.[53]

The temperature dependences of the orbital widths of all three samples are compared between 10 and 300 K in Fig. 17. At 10 K, the (undeconvolved) widths of the $x=0.25$, 0.4, and 0.5 samples are about 0.0008, 0.0028, and 0.004 reciprocal lattice units (r.l.u.), respectively, giving the correlation lengths noted above. There is a clear decrease of orbital domain size as the doping increases from $x=0.25$ to 0.5. A possible explanation for difference between the $x=0.4$ and 0.5 samples follows from the fact that the $x=0.5$ sample is closer to being tetragonal than the $x=0.4$ sample. Specifically, $\zeta(x=0.5)=2(a-b)/a+b=1.48\times10^{-3}$ compared $\zeta(x=0.4)=4.23\times10^{-3}$ at room temperature.[5] In the more tetragonal sample, the a and b domains are more nearly degenerate and the energetic cost of a domain wall is, therefore, reduced.[54] With regard to the difference between the $x=0.25$ sample and the $x=0.4$ and 0.5 samples, we emphasize that the increased doping introduces charge ordering into the orbital lattice and changes the orbital periodicity [compare Figs. 3(a) and 3(b)], and it is not clear that the two situations may be directly compared.

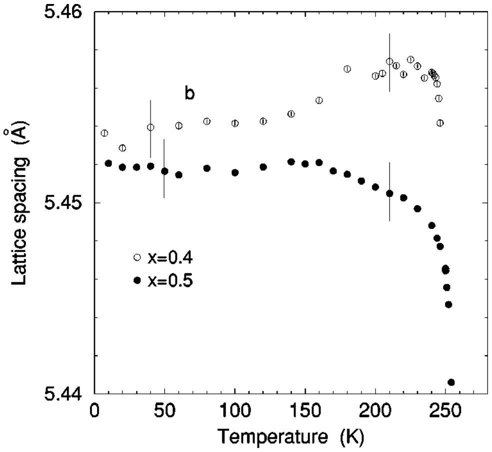

FIG. 18. Temperature dependence of the b-axis lattice constants of the $x=0.4$ (open) and $x=0.5$ (closed) samples.

3. Lattice constants and wavevectors

The temperature dependence of the b-axis lattice constants between 10 and 300 K is shown for the $x=0.4$ and 0.5 samples in Fig. 18. These data were obtained from measurements of the (0,2,0) and (0,4,0) bulk Bragg peaks. As shown in the figure, there is an abrupt change in lattice parameter of both samples at the onset of charge and orbital ordering near 250 K. This is consistent with the formation of both a cooperative Jahn-Teller distortion and a longitudinal lattice distortion as discussed in Sec. V B above. In the $x=0.4$ sample, the lattice constant is approximately constant below $T_0=245$ K, and then decreases slightly at the magnetic ordering temperature ($T_N=170$ K). The lattice constant of the $x=0.5$ sample increases slightly below T_0, and then levels off below T_N. These changes at T_0 and T_N are greatest for the $x=0.4$ sample, which also exhibits the longer-ranged orbital order. This implies that both the orbital- and magnetostriction may be partially compensated at domain boundaries, which occur more frequently in the $x=0.5$ sample. The data obtained for the b-axis lattice constant of the $x=0.5$ sample are in quantitative agreement with results of Jirak *et al.*[27] on a powdered sample.

The temperature dependences of the charge and orbital wavevectors are plotted for the $x=0.25$, 0.4 and 0.5 samples in Fig. 19. The different symbols (detailed in the caption) represent results obtained by x-ray resonant scattering techniques at the (0,1,0) and (0,1/2,0) reflections, and by neutron scattering at the (2,1/2,0) reflection. (The neutron scattering experiments were performed at the NIST Center for Neutron Research, and will be described in detail elsewhere.) All of the wavevectors remain commensurate with the lattice and locked either to (0,1,0) or (0,1/2,0) throughout the ordered phase, independent of temperature to within 0.002 r.l.u. This is in striking disagreement with the results of electron diffraction studies by Chen *et al.*[26] and Jirak *et al.*,[27] in which the orbital order wavevectors were found to change by as

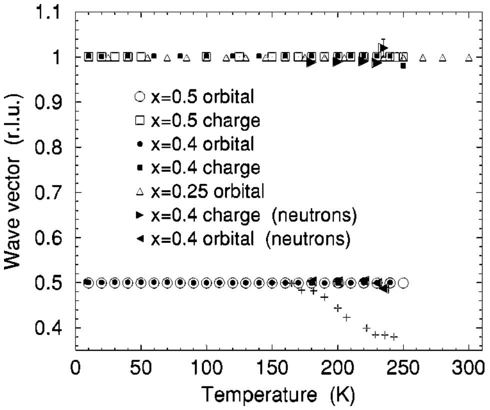

FIG. 19. Temperature dependence of the orbital and charge wavevectors measured in all three samples, by both x-ray and neutron diffraction. Crosses give the results of electron diffraction studies of a sample with $x=0.5$ taken from Ref. 26.

much as 30%. Indeed, Jirak *et al.*[27] suggest the possibility of a devil's staircase in the temperature dependence of the charge order wavevector. It also differs with very recent neutron scattering studies of the (2,1/2,0) reflection by Kajimoto *et al.*[3] For comparison, the results of Chen *et al.*[26] are schematically shown by the crosses in Fig. 19. The origin of the difference between these results and ours is not understood. (See *Note added in proof*).

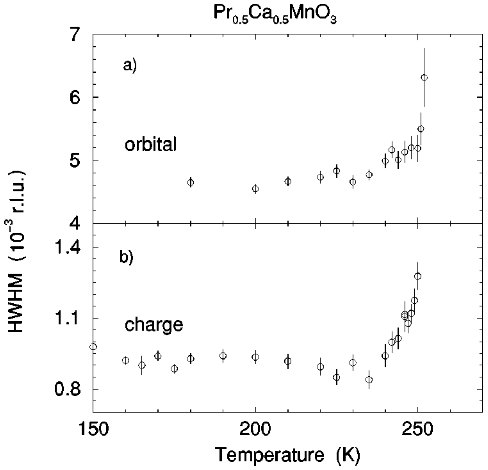

FIG. 21. Temperature dependence of the undeconvolved half widths at half maximum of the scattering at the orbital (0,2.5,0) and charge (0,1,0) reflections of the $x=0.5$ sample.

4. Scattering above the charge- and orbital-ordering temperature

The behavior of the charge and orbital ordering in the vicinity of the phase transition at $T_0=245$ K is illustrated for the $x=0.4$ sample in Fig. 20. Longitudinal scans were taken upon warming of the (0,3,0) reflection in a $\sigma\rightarrow\sigma$ geometry and of the (0,2.5,0) reflection in a $\sigma\rightarrow\pi$ geometry. The peak intensities are plotted on a logarithmic scale between 200 and 280 K in Fig. 20(a). Measurable charge-order fluctuations are observed at much higher temperatures above 245 K than for orbital fluctuations, with weak charge-order scattering still present at 280 K. In contrast, the orbital fluctuations fall off more quickly, and have disappeared by 260 K, at least to within the present counting statistics. The corresponding peak widths are considerably narrower for the charge order than for the orbital order [Fig. 20(b)], that is, the correlation lengths of the charge-order fluctuations are significantly longer than those of the orbital-order fluctuations at any given temperature above $T_0=245$ K. In this regard, it is worth noting that the correlation length of the charge-order must be at least as long as that of the orbital order since the orbital unit cell is defined on the charge-order lattice.

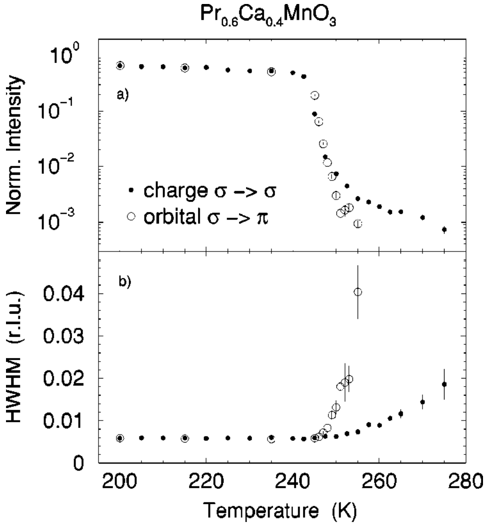

FIG. 20. (a) Temperature dependence of the peak intensities of the (0,3,0) charge-order peak (closed circles) and the (0,2.5,0) orbital-order peak (open circles) of the $x=0.4$ sample. (b) Temperature dependence of the half widths at half maximum.

The picture these data present for the charge and orbital ordering transition in the $x=0.4$ sample is one in which the transition proceeds via local charge-order fluctuations that grow as the transition is approached from above. Long-range charge order is nucleated at the transition temperature. Orbital fluctuations are induced by the charge-order fluctuations and become observable only close to the transition. The coupling mechanism has yet to be fully elucidated, though a quadratic coupling has been suggested by Zhang and Wang,[28] on the basis of a Landau theory, as noted above.

The temperature dependences of the charge- and orbital-order half-widths are plotted between 180 and 300 K for the $x=0.5$ sample in Figs. 21(a) and 21(b). The orbital scattering was characterized in a low-resolution mode with a Cu(220) analyzer in the $\sigma\rightarrow\pi$ geometry. The widths show a clear increase just below the transition; however, the signal is extremely weak and disappears about 1 K above it. The charge-order scattering was characterized using a higher-resolution Ge(111) analyzer. Its width also increases near the transition, however, is always smaller than the smallest value exhibited by the orbital scattering in the ordered phase. Thus, the length scale of the charge-order fluctuations exceeds that of the orbital fluctuations over the narrow temperature range in which both exist. In this sense the data for the $x=0.5$ sample are consistent with the results for the $x=0.4$ sample, although they are neither as convincing nor as clean. Definitive conclusions will require further experiments at a more intense beam line. Preliminary results of such experiments support the suggestions made here. It is worth adding that the orbital scattering observed in the $x=0.25$ sample was not observed to broaden, within experimental errors, at any temperature.

Finally, we note that the narrowing of the orbital reflection in the $x=0.5$ sample below T_0 is consistent with the behavior previously seen in a number of diverse systems for which disorder prevents the particular order parameter reaching its long-range ordered ground state. Examples include magnetic order in dilute antiferromagnets in applied fields (see, for example Ref. 55) and doped spin-Peierls systems.[56] In these two examples, the common phenomenology appears to be rapidly increasing time scales as the transition is approached, such that the system is not able to fully relax and reach equilibrium. As the temperature is reduced further, equilibration times become longer than experimental measuring times and the system freezes in a metastable glasslike state. It is possible that similar phenomena underlie the behavior observed here. As noted above, the disorder is greater in the $x=0.5$ sample. In this regard, we note that the line shape of the orbital reflection, a Lorentzian squared, is the same as that observed in the dilute antiferromagnets. It may be derived from exponentially decaying real-space correlations.

VI. MAGNETIC FIELD DEPENDENCE

An intriguing property of the perovskite manganites is the existence of colossal magnetic resistance behavior in an applied magnetic field. The transition to a metallic phase involves the delocalization of the Mn e_g electrons, which leads to the destruction of static charge and orbital ordering. That this transition can be driven by a magnetic field in $\mathrm{Pr}_{1-x}\mathrm{Ca}_x\mathrm{MnO}_3$ was first demonstrated by Tomioka *et al.*[33] It is an interesting question whether the same phenomenology of the transition discussed above applies when the transition is driven at fixed temperature and the fluctuations are activated by a magnetic field. We have carried out studies of the transition at two temperatures, $T=30$ and 200 K, with critical fields of $H_0=6.9(1)$ and 10.4 T, respectively.[33] The field dependence of the charge and orbital intensities of the $x=0.4$ sample taken at $T=30$ K are illustrated in Fig. 22. The intensities of the (0,3,0) and (0,2.5,0) reflections exhibit identical field dependences below the transition. Above the transition, the charge-order fluctuations are markedly stronger than the orbital fluctuations. A similar behavior was also observed at $T=200$ K, i.e., charge-order fluctuations were observed at fields for which orbital fluctuations were no longer observable (see inset, Fig. 22). From this it appears that the disorder transition is driven by charge-order fluctuations for both the temperature- and field-driven cases. We note that as a result of experimental constraints it was only possible to measure the charge and orbital ordering at a photon energy of 8 keV in an applied magnetic field. The corresponding nonresonant intensities are sufficiently weak above 6.5 T that it was not possible to obtain reliable values of the half-widths.

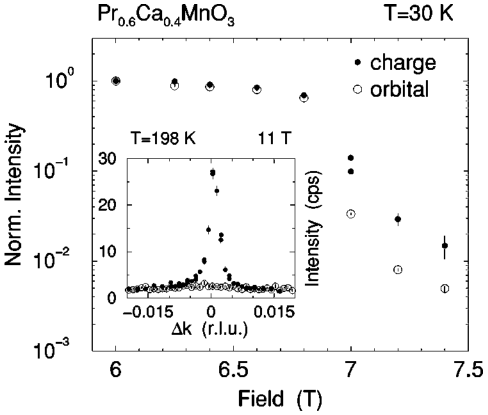

FIG. 22. Magnetic field dependence of the charge- and orbital-ordering intensities of the $x=0.4$ sample obtained at 30 K. Inset: Charge- and orbital-order superlattice reflections at $T=198$ K and 11 T.

VII. CONCLUSIONS

This paper describes a systematic study of the charge and orbital ordering in the manganite series $\mathrm{Pr}_{1-x}\mathrm{Ca}_x\mathrm{MnO}_3$ with $x=0.25$, 0.4, and 0.5. The temperature dependence of the charge and orbital ordering was characterized in each sample, including the correlation lengths, wavevectors, and lattice constants. It was found that the charge and orbital ordering are strictly commensurate with the lattice in all three samples, although very recent studies of the $x=0.5$ sample carried out at 30 keV also reveal an incommensurate phase. We do not understand the origin of these discrepancies. High-Q-resolution scans revealed that long-range orbital order is never established in the $x=0.4$ and 0.5 samples, a result that makes connections with the observation of finite Mn^{3+} magnetic domains in neutron diffraction studies of $\mathrm{Pr_{0.5}Ca_{0.5}MnO_3}$ and $\mathrm{La_{0.5}Ca_{0.5}MnO_3}$. We suggest that the orbital domains observed here represent the antiphase magnetic domain walls responsible for destroying the Mn^{3+} magnetic order. The observation of such an orbital glasslike state in two such materials suggests that such phenomena may be common in manganites, at least those with the CE-type charge and orbital structure. Above the charge- and orbital-ordering temperature T_0, we found that the charge-order fluctuations are more highly correlated than the orbital-order fluctuations. This suggests that charge order drives orbital order in these systems. In addition, we reported on the destruction of charge and orbital ordering in the $x=0.4$ sample by the application of a magnetic field. A similar phenomenology was found for increasing field as was found for increasing temperature. Finally, the polarization and azimuthal dependence of the resonant charge and orbital ordering at the Mn K edge is found to be qualitatively consistent with the predictions of a simple model in which the $4p$ levels are split in the orbitally ordered phase. The experiments do not distinguish among more sophisticated treatments of the electronic structure, whether in atomic or band limits. Of note is the discovery of a longitudinal lattice modulation in the $x = 0.4$ and 0.5 samples with scattering at both the charge and orbital wavevectors. The presence of such a component of the modulation represents a refinement of earlier models in which the displacement was assumed to be purely transverse, following work on $La_{0.5}Ca_{0.5}MnO_3$ and $Pr_{0.5}Ca_{0.5}MnO_3$.

Note added in proof. We are intrigued to report that very recent x-ray scattering experiments we have carried out on the $x=0.5$ sample have revealed incommensurate ordering of the orbital order scattering starting at about 220 K, and qualitatively consistent with earlier electron diffraction results. These experiments were performed using 32 keV incident x-ray energies, but otherwise reproduced the sample conditions described in the paper. It's clear that still further experiments are required on this sample to understand how it may exhibit two different behaviors. Similar high energy experiments performed on the $x=0.4$ sample were consistent with resonant x-ray scattering data below the transition, which is presented here.

We acknowledge helpful conversations with S. Ishihara, D.J. Khomskii, S. Maekawa, A.J. Millis, and G. A. Sawatzky. We thank Jeff Lynn for his help with the neutron scattering experiments performed at NIST. The work at Brookhaven, both in the Physics Department and at the NSLS, was supported by the U.S. Department of Energy, Division of Materials Science, under Contract No. DE-AC02-98CH10886, and at Princeton University by the NSF under Grant No. DMR-9701991. Support from the Ministry of Education, Science and Culture, Japan, by the New Energy and Industrial Technology Development Organization (NEDO), and by the Core Research for Evolution Science and Technology (CREST) is also acknowledged. Work at the CMC beam lines is supported, in part, by the Office of Basic Energy Sciences of the U.S. Department of Energy and by the National Science Foundation, Division of Materials Research. Use of the Advanced Photon Source was supported by the Office of Basic Energy Sciences of the U.S. Department of Energy under Contract No. W-31-109-Eng-38.

---

[1] *Physics of Manganites*, edited by T. A. Kaplan and S. D. Mahanti (Kluver, Academic, 1999).

[2] E. Wollan and W. Koehler, Phys. Rev. **100**, 545 (1955).

[3] R. Kajimoto, H. Yoshizawa, Y. Tomioka, and Y. Tokura, cond-mat/0009041; Phys. Rev. B **63**, 212407 (2001).

[4] J. Goodenough, Phys. Rev. **100**, 555 (1955).

[5] Z. Jirak, S. Krupica, Z. Simsa, M. Dlouha, and S. Vratislav J. Magn. Magn. Mater. **53**, 153 (1985).

[6] P. G. Radaelli, D. E. Cox, M. Marezio, and S.-W. Cheong, Phys. Rev. B **55**, 3015 (1997).

[7] Y. Murakami, H. Kawada, H. Kawata, M. Tanaka, T. Arima, Y. Moritomo, and Y. Tokura, Phys. Rev. Lett. **80**, 1932 (1998).

[8] Y. Murakami, J. P. Hill, D. Gibbs, M. Blume, I. Koyama, M. Tanaka, H. Kawata, T. Arima, Y. Tokura, K. Hirota, and Y. Endoh, Phys. Rev. Lett. **81**, 582 (1998).

[9] S. Ishihara and S. Maekawa, Phys. Rev. Lett. **80**, 3799 (1998).

[10] M. Fabrizio, M. Altarelli, and M. Benfatto, Phys. Rev. Lett. **80**, 3400 (1998).

[11] I. S. Elfimov, V. I. Anisimov, and G. A. Sawatzky, Phys. Rev. Lett. **82**, 4264 (1999).

[12] Y. Endoh, K. Hirota, S. Ishihara, S. Okamoto, Y. Murakami, A. Nishizawa T. Fukada, H. Kimura, H. Nojiri, K. Kaneko, and S. Maekawa, Phys. Rev. Lett. **82**, 4328 (1999).

[13] P. Fulde, J. Phys. Soc. Jpn. **5**, 154 (2000).

[14] P. Wochner *et al.* (unpublished).

[15] M. v. Zimmermann, J. P. Hill, D. Gibbs, M. Blume, D. Casa, B. Keimer, Y. Murakami, Y. Tomioka, and Y. Tokura, Phys. Rev. Lett. **83**, 4872 (1999).

[16] L. Paolosini, C. Vettier, F. de Bergevin, F. Yakhou, D. Mannix, A. Stunault, W. Neubeck, M. Altarelli, M. Fabrizio, P. A. Metcalf, and J. M. Honig, Phys. Rev. Lett. **82**, 4719 (1999).

[17] H. Nakao *et al.* (unpublished).

[18] B. Keimer, D. Casa, A. Ivanov, J. W. Lynn, M. v. Zimmermann, J. P. Hill, D. Gibbs, Y. Taguchi, and Y. Tokura, Phys. Rev. Lett. **85**, 3946 (2000).

[19] Y. Wakabayashi, Y. Murakami, I. Koyama, T. Kimura, Y. Tokura, Y. Moritomo, K. Hirota, and Y. Endoh, J. Phys. Soc. Jpn. **69**, 2731 (2001).

[20] Y. Tanaka, T. Inami, T. Wakamura, H. Yamauchi, H. Onoderon, K. Ohoyama, and Y. Yamaguchi, J. Phys.: Condens. Matter **11**, L505 (1999).

[21] K. Hirota, N. Oumi, T. Matsumura, H. Nakao, Y. Wakabayashi, Y. Murakami, and Y. Endoh, Phys. Rev. Lett. **84**, 2706 (1999).

[22] K. Nakamura, T. Arima, A. Nakazawa, Y. Wakabayashi, and Y. Murakami, Phys. Rev. B **60**, 2425 (2000).

[23] P. Hatton, Bulletin No. 11, Stefan University (1999), p. 337 (unpublished).

[24] M. Benfatto, Y. Joly, and C. R. Natoli, Phys. Rev. Lett. **83**, 636 (1999).

[25] S. Ishihara and S. Maekawa, Phys. Rev. B **58**, 13 442 (1998).

[26] C. H. Chen, S. Mori, and S.-W. Cheong, Phys. Rev. Lett. **83**, 4792 (1999).

[27] Z. Jirak, F. Damay, M. Hervieu, C. Martin, B. Raveau, G. Andre, and F. Bouree, Phys. Rev. B **61**, 1181 (2000).

[28] F. Zhang and Z. D. Wang, Phys. Rev. B **61**, 3192 (2000).

[29] P. G. Radaelli, D. E. Cox, L. Capogna, S.-W. Cheong, and M. Marezio, Phys. Rev. B **59**, 14 440 (1999).

[30] R. Wang, J. Gui, Y. Zhu, and A. Moodenbaugh (unpublished).

[31] C. H. Chen and S.-W. Cheong, Phys. Rev. Lett. **76**, 4042 (1990).

[32] Y. Okimoto, Y. Tomioka, Y. Onose, Y. Otsuka, and Y. Tokura, Phys. Rev. B **57**, R9377 (1998).

[33] Y. Tomioka, A. Asamitsu, H. Kuwahara, Y. Moritomo, and Y. Tokura, Phys. Rev. B **53**, 1689 (1996).

[34] Y. Tokura and Y. Tomioka, J. Magn. Magn. Mater. **200**, 1 (1999).

[35] D. Gibbs, M. Blume, D. R. Harshman, and D. B. McWhan, Rev. Sci. Instrum. **60**, 1655 (1988).

[36] T. Mizokawa, D. I. Khomskii, and G. A. Sawatzky, Phys. Rev. B **61**, R3776 (2000).

[37] T. Mizokawa, D. I. Khomskii, and G. A. Sawatzky, Phys. Rev. B **63**, 024403 (2001).

[38] T. Hotta and E. Dagotto, Phys. Rev. B **61**, 11879 (2000).

[39] M. Blume, in *Resonant Anomalous X-Ray Scattering*, edited by

G. Materlik, C. J. Sparks, and K. Fischer (North-Holland, Amsterdam, 1991), p. 495.

[40] J. P. Hannon, G. T. Trammell, M. Blume, and D. Gibbs, Phys. Rev. Lett. **61**, 1245 (1988).

[41] P. Benedetti, J. V. D. Brink, E. Pavarini, A. Vigliante, and P. Wochner, Phys. Rev. B **63**, 060408(R) (2001).

[42] M. Takahashi, J. Igaraski, and P. Fulde, J. Phys. Soc. Jpn. **68**, 2530 (1999).

[43] H. Yoshizawa, H. Kawano, Y. Tomioka, and Y. Tokura, Phys. Rev. B **52**, R13 145 (1995).

[44] V. Kiryukhin, D. Casa, J. P. Hill, B. Keimer, A. Vigliante, Y. Tomioka, and Y. Tokura, Nature (London) **386**, 813 (1997).

[45] Y. Murakami *et al.* (unpublished).

[46] S. Ishihara and S. Maekawa, Phys. Rev. B **62**, 5690 (2000).

[47] M. Takahashi, J. Igaraski, and P. Fulde, J. Phys. Soc. Jpn. **69**, 1614 (2000).

[48] D. E. Cox, P. G. Radaelli, M. Marezio, and S.-W. Cheong, Phys. Rev. B **57**, 3305 (1998).

[49] C. S. Nelson, M. v. Zimmermann, Y. J. Kim, J. P. Hill, D. Gibbs, V. Kiryukhin, T. Y. Koo, S-W. Cheong, D. Casa, B. Keimer, Y. Tomioka, Y. Tokura, T. Gog, and C. Venkataraman, Phys. Rev. B **64**, 174405 (2001).

[50] Note that the description in terms of Mn^{3+} (d^4) and Mn^{4+} (d^3) ions is qualitative. There is nothing in our data that requires the hole to reside on the Mn site in its entirety, i.e., it is possible that some degree of charge transfer with the oxygen orbitals occurs such that the electronic configuration is an admixture of d^3 and $d^4\underline{L}$ on the ‘‘Mn^{4+}’’ sites. This also produces an edge shift because of the change in the environment of the Mn site. What our data do require is that the ‘‘Mn^{4+}’’ sites are ordered in a regular pattern, as described throughout the paper. It is not clear how this description can be reconciled with the mixed valency interpretation of XANES data, e.g., C. H. Booth *et al.*, Phys. Rev. B **57**, 10 440 (1998) (Ref. 52).

[51] G. Ice, C. J. Sparks, and L. B. Shaffer, in *Resonant Anomalous X-Ray Scattering*, edited by G. Materlik, C. J. Sparks, and K. Fischer (North-Holland, Amsterdam, 1991), p. 495.

[52] C. H. Booth, F. Bridges, G. H. Kwei, J. M. Lawrence, A. L. Cornelius, and J. J. Neumeier, Phys. Rev. B **57**, 10 440 (1998).

[53] R. Kajimoto, T. Kakeshita, Y. Oohara, H. Yoshizawa, Y. Tomioka, and Y. Tokura, Phys. Rev. B **58**, R11 837 (1998).

[54] A. Millis (private communication).

[55] J. P. Hill, Q. Feng, R.-J. Birgeneau, and T. R. Thurston, Z. Phys. B: Condens. Matter **92**, 285 (1993).

[56] Y. J. Wang, V. Kiryukhin, R. J. Birgeneau, T. Masuda, I. Tsukada, and K. Uchinokura, Phys. Rev. Lett. **83**, 1676 (1999).